

Article

Correlation between Frequency-Divided Magnetic Field and Channel-Base Current for Rocket-Triggered Lightning

Yanfeng Fan ¹, Yang Zhang ^{1,*}, Weitao Lyu ¹, Ying Ma ¹, Bin Wu ¹, Qi Qi ¹, Dong Zheng ¹, Gaopeng Lu ^{2,3} and Ankun Wu ⁴

¹ State Key Laboratory of Severe Weather & CMA Key Laboratory of Lightning, Chinese Academy of Meteorological Sciences, Beijing 100081, China; fanyf@cma.gov.cn (Y.F.); wtylu@cma.gov.cn (W.L.); may@cma.gov.cn (Y.M.); wubin@cma.gov.cn (B.W.); qiqi@cma.gov.cn (Q.Q.); zhengdong@cma.gov.cn (D.Z.)

² School of Earth and Space Sciences, University of Science and Technology of China, Hefei 230026, China; gplu@ustc.edu.cn

³ Key Laboratory of Atmospheric Optics, Anhui Institute of Optics and Fine Mechanics, Hefei Institutes of Physical Science, Chinese Academy of Sciences, Hefei 230031, China

⁴ Guizhou Meteorological Disaster Prevention Technology Center, Guiyang 550081, China; wuankun340519@cma.cn

* Correspondence: zhangyang@cma.gov.cn

Abstract: Different discharge processes of triggered lightning can radiate electromagnetic signals with different frequency bands. During the triggered-lightning experiment conducted at the Field Experiment Base on Lightning Sciences of China Meteorological Administration (CMA-FEBLS), three magnetic field (*B*-field) antennas with different frequency responses were deployed at about 80 m from the rocket-launching site. By using the synchronous observations, the quantitative relationship between the close-range *B*-field measurement and the channel-base current at different stages of triggered lightning were established in the investigation. The initial continuous current (ICC) waveform can be reconstructed by numerically integrating the *B*-field signals measured with the dB/dt antenna. However, the slow variations of ICC cannot be retrieved by the *B*-field signals measured with the LF-MF antenna because the antenna bandwidth cannot cover a frequency below 500 Hz. The *B*-field signals of the return stroke measured with the low-sensitivity antenna can be simulated by the MTL return-stroke model, and the *B*-field signal shows a fairly good consistency with the return-stroke current. The analyses suggest that the current waveform of the natural return stroke that occurred within 1.5 km can be retrieved, or at least its peak value can be estimated by using the *B*-field measurements.

Keywords: rocket-triggered lightning; frequency-divided *B*-field antenna; initial continuous current; return stroke



check for updates

Citation: Fan, Y.; Zhang, Y.; Lyu, W.; Ma, Y.; Wu, B.; Qi, Q.; Zheng, D.; Lu, G.; Wu, A. Correlation between Frequency-Divided Magnetic Field and Channel-Base Current for Rocket-Triggered Lightning. *Remote Sens.* **2023**, *15*, 3902. <https://doi.org/10.3390/rs15153902>

Academic Editor: Yuriy Kuleshov

Received: 18 June 2023

Revised: 3 August 2023

Accepted: 3 August 2023

Published: 7 August 2023



Copyright: © 2023 by the authors. Licensee MDPI, Basel, Switzerland. This article is an open access article distributed under the terms and conditions of the Creative Commons Attribution (CC BY) license (<https://creativecommons.org/licenses/by/4.0/>).

1. Introduction

As one of the most important physical parameters of lightning, the lightning current is essential for the research of lightning physics, lightning damaging effects, and its protective techniques [1–4]. However, it is difficult to obtain the current waveforms of natural lightning flashes for the random characteristics of lightning discharge. By providing a relatively fixed discharge path, rocket-triggered lightning can create good opportunities for the measurements of lightning-current waveform [5–7]. Specifically, the coaxial shunt or Pearson coil with different settings of measuring range can be installed at the base of the discharge path to conduct the direct or indirect measurements of a lightning current. The triggered-lightning flash consists of several stages with different discharge characteristics. A rocket tailing a grounded metal wire is launched towards the thundercloud at a velocity of 100–200 m/s [8–10]; when the potential gradient around the wire tip is sufficiently strong, the attempted breakdown into ambient air will occur, exhibiting some transient

current pulses or called “precursors” [11] in the current measurements. As the height of the rocket increases, the attempted breakdown can transform into the sustained upward leaders with the typical current amplitude of about tens to more than 100 A [12,13], and then, the initial continuous current (ICC) appears, indicating the onset of a continuous charge transfer from thundercloud to ground [14]. The ICC is the main process of charge transfer in triggered lightning, after that, often accompanied by subsequent return strokes.

All the sub-processes of triggered lightning can be divided into two categories, including the impulsive discharge lasting several to dozens of microseconds and the continuous discharge lasting tens to hundreds of milliseconds. In addition to the measurements of channel-base current, another important advantage for triggering lightning is the ability to perform close-range electromagnetic field observations. Lightning electromagnetic signals are closely related to the lightning current, and hence, the frequency-spectrum distribution for different categories of discharge processes varies greatly. Moreover, the quantitative relationship between the close-range electromagnetic field and the channel-base current is affected by the bandwidth of the electromagnetic antenna. In terms of component composition, the electric field (E -field) contains an electrostatic component associated with an electric charge, the induction component associated with the current and the radiation component associated with the change of the current with time [15]. The magnetic field (B -field) contains only the induction component and the radiation component. Therefore, it is easier to establish the quantitative relationship between the magnetic field and the channel-base current. During the SHAndong Triggering Lightning Experiment (SHATLE) [16,17], Fan et al. [18,19] measured the B -field pulses associated with the sustained upward leaders by using a low-frequency (LF) magnetic antenna at 78 m from the rocket-launching site and found the correlation between the B -field pulse and the channel-base current by a transmission-line (TL) model. However, the B -field signals radiated by ICC have no correlation with the associated current in terms of waveform, since the frequency band of ICC is mainly in the dB/dt portion of the antenna. Based on that, Lu et al. [20] reconstructed the ICC waveform by numerically integrating the B -field signals measured with the LF magnetic antenna during the SHATLE campaign, but the validity of this method should be verified further. As for the return stroke, the correlation between the channel-base current and its close-range B -field radiation has not been analyzed, since the sensitivity of the B -field antenna used before was too large to acquire unsaturated waveforms. In order to analyze the relationship between the current and B -field radiations of all sub-processes of triggered lightning, it is necessary to conduct close-range B -field observations with multi-gains and different frequency bands.

In the summer of 2022, three B -field antennas with different frequency responses were deployed at about 80 m from the rocket-launching site of the Field Experiment Base on Lightning Sciences, China Meteorological Administration (CMA-FEBLS), which was formerly known as Guangdong Comprehensive Observation Experiment on Lightning Discharge (GCOELD) [21,22]. According to the main frequency ranges and amplitudes of these curves, the three-frequency-divided B -field antennas are named LF-MF antenna, dB/dt antenna, and low-sensitivity antenna, respectively. The LF-MF antenna can be used to measure the broadband B -field signals radiated by upward leaders. The dB/dt antenna aims at the B -field signals of long continuous discharge [20]. The low-sensitivity antenna can obtain the unsaturated B -field signals caused by return strokes. Based on the measurements of the three B -field antennas, the quantitative relationship between the close-range B -field signals and the channel-base current at different stages of triggered lightning is analyzed in this paper. Under certain conditions, the correlation established during the triggered lightning can be used to retrieve the current waveform of natural lightning, or at least estimate the current peak value.

2. Measurements and Data

The triggered-lightning experiment of CMA-FEBLS was conducted in Guangdong Province starting in 2006, and the detailed arrangements of the experiment were described by Zheng et al. [21] and Zhang et al. [22]. The experimental data analyzed in this paper, mainly including the frequency-divided B -fields and channel-base current, were obtained at 07:59:48 UTC on 7 July 2022 of the CMA-FEBLS campaign. Figure 1 shows the schematic diagram for the measurements of these experimental data. In particular, the channel-base current was measured by a 1-m Ω coaxial shunt with the bandwidth of 0–3.2 MHz, which was installed at the bottom of the discharge path; three B -field antennas with different frequency responses were deployed at about 80 m from the rocket-launching site (at 23.64°N, 113.60°E). The output from the shunt was fed into two HBM HV6600 transmission systems, and the measurable current ranges were separately set to ± 50 kA and ± 2 kA. Then the signals from the transmission systems were sent via a 100 m fiber-optic cable to the control room for recording. The B -field signals were transmitted through a 10 m coaxial cable to the control room, and the conducting shield of coaxial cable was grounded at both ends. Both channel-base current and magnetic signals were sampled at 10 MHz with 12-bit amplitude resolution by using a Yokogawa DL850 digitizing oscilloscope in the control room.

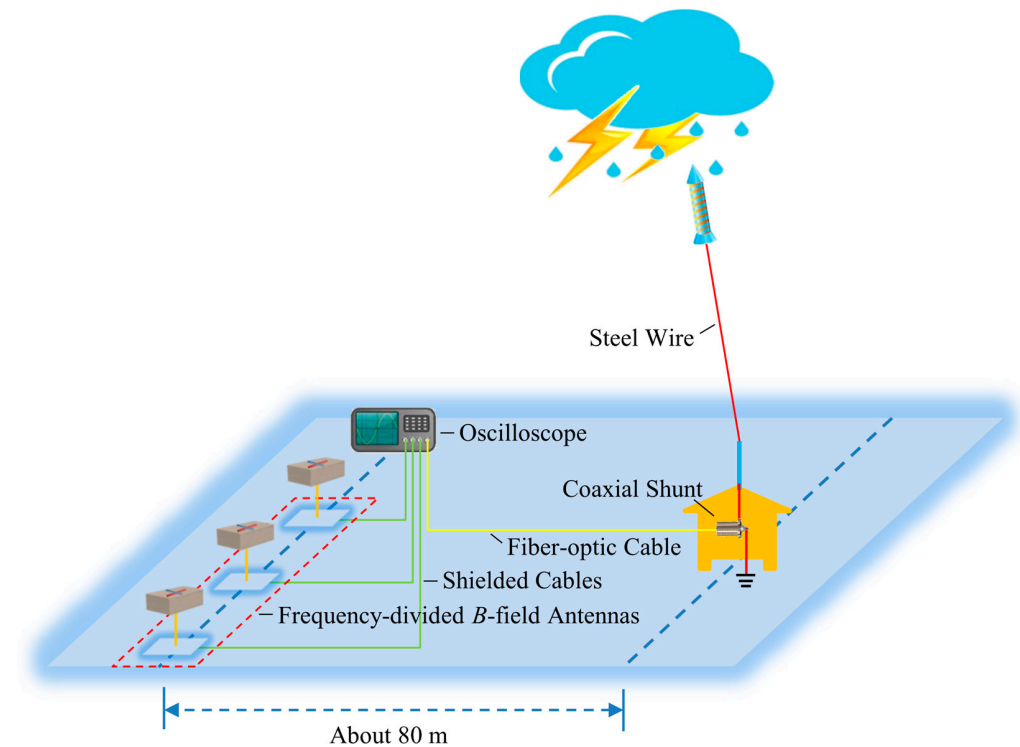


Figure 1. Schematic diagram for the measurements of frequency-divided B -fields and channel-base current for the triggered lightning at 07:59:48 UTC on 7 July 2022.

Frequency responses of the frequency-divided B -field antennas mentioned above are shown in Figure 2. According to the main frequency ranges and amplitudes obtained from the calibration curves, the three frequency-divided B -field antennas are named LF-MF antenna (blue line), dB/dt antenna (red line) and low-sensitivity antenna (green line), respectively. The LF-MF antenna with the 3-dB bandwidth set to 20 kHz to 1.2 MHz was used to measure the B -field radiation generated by the upward positive leader (UPL) of triggered lightning at CMA-FEBLS since 2020. The dB/dt antenna is designed to obtain lower frequency signals in lightning discharge, and hence, it is the dB/dt portion (from 40 Hz to 8.5 kHz), but not the 3-dB portion (from 8.5 kHz to 52 kHz), that is used as the main operating band of the antenna in the experiment. The bandwidth of dB/dt

portion ranges from super low frequency (SLF) to very low frequency (VLF). As for the low-sensitivity antenna, its designed antenna gain (0.000044 V/nT) is three to four orders of magnitude smaller than the other two antennas (0.06 V/nT for dB/dt antenna and 0.1 V/nT for LF-MF antenna), in order to obtain the unsaturated B -field signals of return strokes.

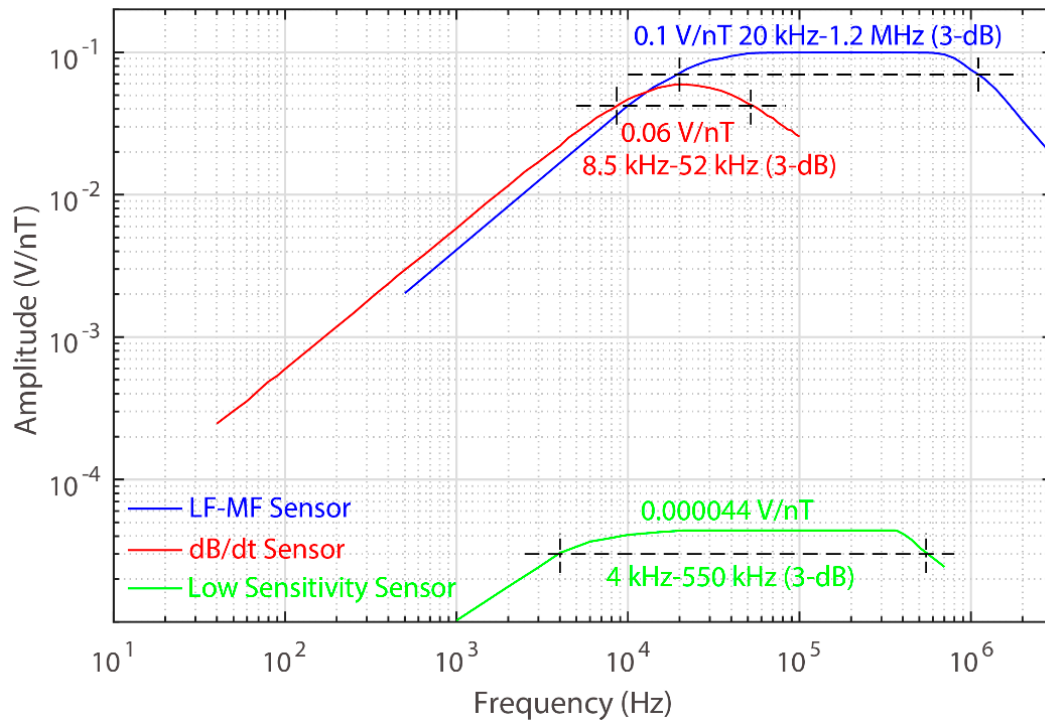


Figure 2. Frequency responses of the frequency-divided B -field antennas used in the triggered-lightning experiment of CMA-FEBLS.

3. Analyses and Results

3.1. Frequency Spectrum for Triggered-Lightning Discharge Processes with Different Temporal Scales and Correspondence with the Bandwidth of B -Field Antenna

As mentioned above, all the sub-processes of triggered lightning can be divided into two categories, i.e., the impulsive discharge and the continuous discharge. The impulsive discharge, such as upward leaders and return strokes, usually lasts several to dozens of microseconds, but with different discharge intensities. The continuous discharge, like ICC and the continuous current after return strokes, can last tens to hundreds of milliseconds. The frequency-spectrum distribution of B -field signals radiated by different categories of discharge processes varies greatly. Taking the typical waveforms of the two types of discharge processes for an example, Figure 3 shows the frequency spectrums of ICC and one return stroke obtained at 07:59:48 UTC on 7 July 2022 of the CMA-FEBLS campaign. For the sake of understanding the measurements, the bandwidth ranges of the three B -field antennas used in the experiment are marked by vertical dashed lines with different colors in Figure 3.

It can be seen that the resolution of frequency-spectrum analysis for ICC is much higher than the return stroke, since ICC lasts longer than the return stroke, and more sampling points of ICC can be used for fast Fourier-transform analysis. In particular, the lowest frequency point for the return stroke is even above 600 Hz, but actually, the frequency components below 600 Hz are included. Note that the flat parts beginning approximately at 10 kHz for ICC and at 1 MHz for the return stroke separately are from the background noise. The initial frequency of the noise level for the return stroke is much higher than for ICC, indicating that the return stroke contains many more components with higher frequency than ICC. As shown in Figure 3, the dB/dt antenna used in our experiment covers the main frequency spectrum of ICC, and only the signals with a very

narrow spectrum below 40 Hz are filtered. For the low-sensitivity antenna designed for the return stroke, its upper frequency limit approaches the noise level, but its lower frequency limit cannot cover the lower frequency components of the signal. Hence, the B -field signals measured by the low-sensitivity antenna can be equivalent to passing through a high-pass filter with an upper cutoff frequency of 4 kHz.

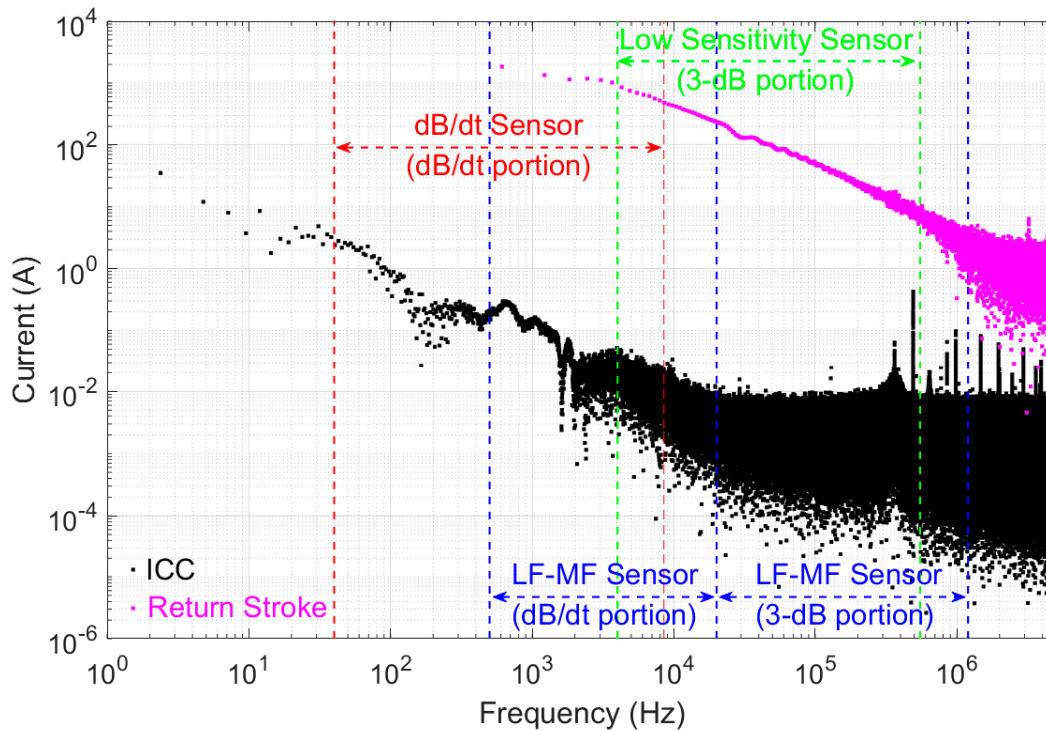


Figure 3. Frequency spectrums of ICC and one return stroke obtained at 07:59:48 UTC on 7 July 2022 of the CMA-FEBLS campaign and the bandwidth ranges of the three B -field antennas used in the experiment.

3.2. Correlation between dB/dt Measurements and Initial Continuous Current

According to Lu et al. [20], the ICC waveform along the lightning path can be reconstructed by numerically integrating the dB/dt magnetic signal recorded at close range, i.e.,

$$I(t) = \beta(t) \int_{t'=t_0}^t \frac{dB}{dt'} dt' \quad (1)$$

where $\beta(t)$ is the conversion coefficient at time t , and $\frac{dB}{dt'}$ is the dB/dt magnetic signal recorded at a certain time. This method is developed on the basis of three factors: first of all, the discharge frequency is mainly in the dB/dt portion of the antenna; secondly, the associated B -field signal is dominated by the induction component so that it is approximately proportional to the current along the lightning channel; thirdly, the conversion coefficient can be treated as a constant, which does not vary considerably with time. However, the validity of this method has not been verified since its first implementation in 2018, let alone examined in the triggered lightning experiment at different sites.

Figure 4 shows the time-resolved current and B -field waveforms recorded for the triggered lightning at 07:59:48 UTC on 7 July 2022 of the CMA-FEBLS campaign. The current waveform (Figure 4a) is obtained by the shunt with a transmission range of ± 2 kA, and thus, the return strokes and M-components after ICC are heavily saturated. The B -field waveforms shown in Figure 4b,c are acquired by the LF-MF antenna and dB/dt antenna. As analyzed above, the frequency of ICC is mainly in the dB/dt portion of these two antennas, which makes the B -field waveform associated with the ICC have no similarity to the ICC

waveform. In addition, Figure 5 shows the discharge-channel image of this triggered lightning, which is captured at about 1.9 km away from the rocket-launching site with a frame rate of 15 fps. Hence, it cannot provide the details of the lightning development, but only the general shape of the lightning channel. From the channel along the trace of steel wire that is approximately perpendicular to the ground, it can be estimated that the triggered lightning is initiated at about 370 m above ground level. Note that, for the B -field radiation received at close range, the signal is closely related to the lower part of the lightning channel, i.e., the B -field signal makes little change in the increase of the lightning channel, as long as the lightning-initiation height is high enough. This is the key factor to ensure that the conversion coefficient can be treated as a constant.

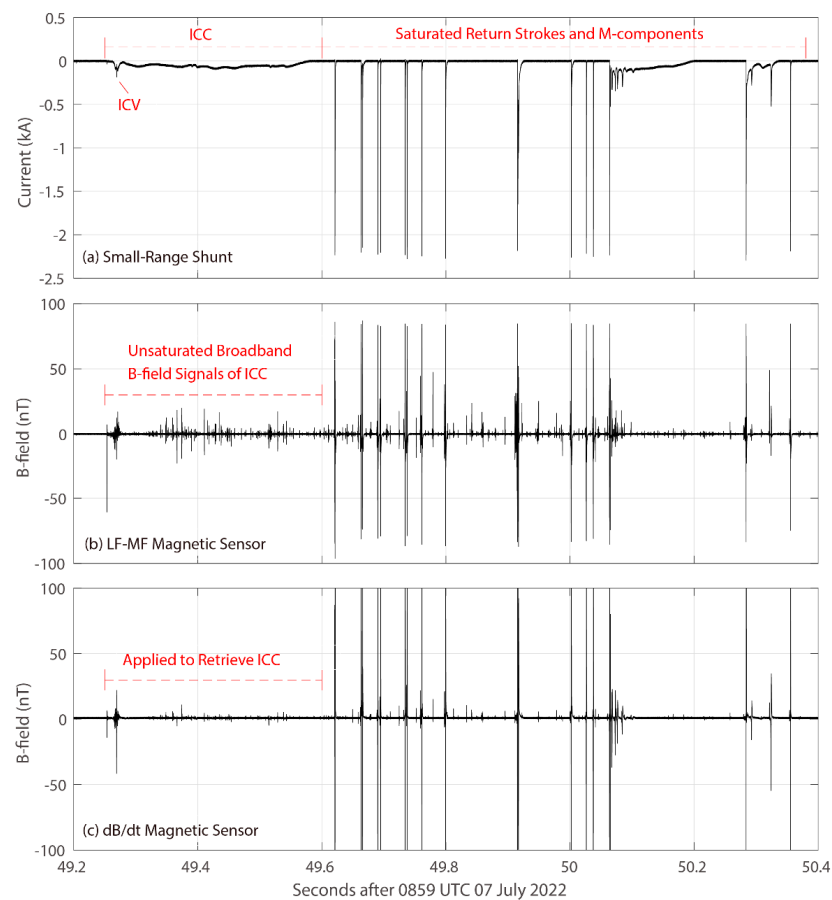


Figure 4. (a) Small-range current measured by the shunt, B -field waveforms obtained by (b) LF-MF antenna and (c) dB/dt antenna for the triggered lightning at 07:59:48 UTC on 7 July 2022 of the CMA-FEBLS campaign.

With the method described above, the B -field signals recorded by the dB/dt antenna at 80 m range are numerically integrated to reconstruct the current waveform along the lightning channel (red waveform in Figure 6) and are compared with the channel-base current as measured by the shunt (black waveform in Figure 6). As the most complex part of the ICC waveform, the reconstruction results of the initial current variation (ICV) can verify the effectiveness of this method. Therefore, the inset in Figure 6 shows the zoomed view of the ICV for the convenience of comparison. In general, it can be seen that the current waveform retrieved from the measurements of the dB/dt antenna shows fairly good consistency with the channel-base current recorded with the shunt. However, for the part of the ICC frequency that is close to DC, the inversion result appears a slight deviation (i.e., after 49.55 s as shown in Figure 6), which is due to the signal loss of the frequency below 40 Hz. The conversion coefficient in the case (0.002 A/nT) is consistent with that in the SHATLE campaign, even though the tortuosity of the channel above the trace of

steel wire differs a great deal in different triggered lightning flashes. The result confirms that the conversion coefficient is dominated by the distance between the dB/dt antenna and the rocket-launching site in the experiment, and the shape of lightning channel above the vertical grounded portion has little effect on it in the range of the triggered-lightning initiation height. Note that the noise level for the retrieved waveforms is much lower than that of the shunt measurement since the B -field measurement noise with random distribution is cancelled mutually during the numerical integration.

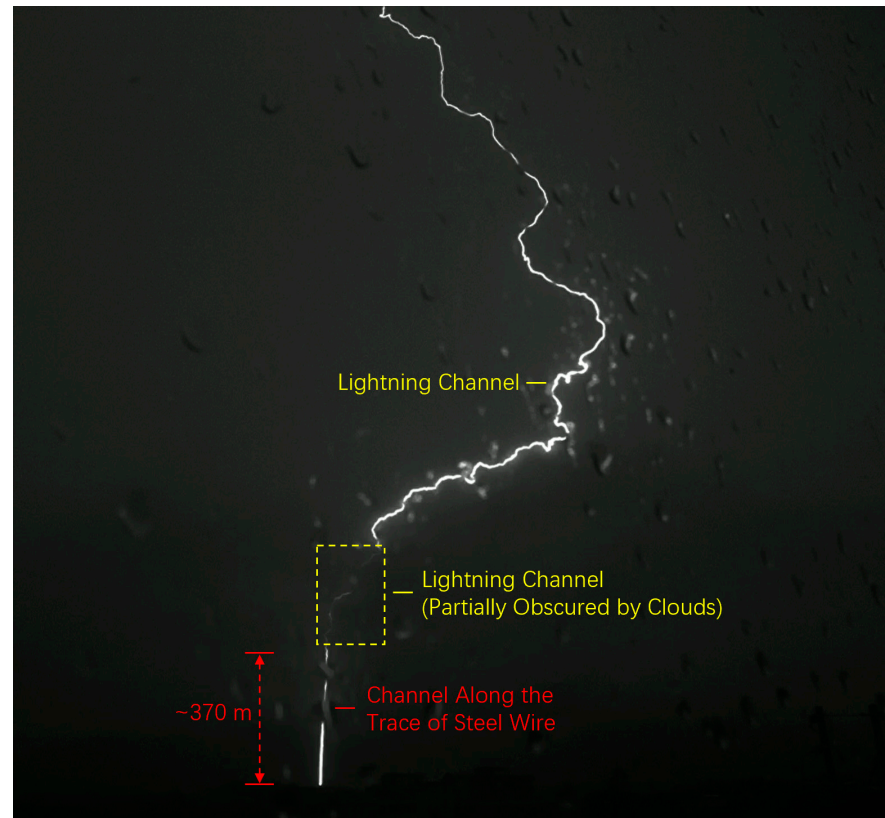


Figure 5. Discharge-channel image captured at about 1.9 km away from the rocket-launching site for the triggered lightning at 07:59:48 UTC on 7 July 2022 of the CMA-FEBLS campaign.

3.3. The B -Field Radiation of the Return Stroke at Close Range

Figure 7 presents the channel-base current obtained by the shunt with the transmission range of ± 50 kA (Figure 7a) and the B -field waveforms acquired by the low-sensitivity antenna (Figure 7b). Both the current and B -field waveforms associated with the return strokes and M-components are well recorded without or with little saturation, but the waveforms associated with ICC are unrecognizable in the measurements.

The transmission line (TL) model has been widely used to calculate the electromagnetic fields radiated by the lightning-return stroke. In this model, the return-stroke current propagates along the lightning channel with constant speed and without any distortion. The TL model can be modified by allowing the current amplitude to decrease with height while maintaining its original shape. In this paper, we assume that the return-stroke current amplitude decays in a linear way along the lightning channel (i.e., MTL model) [23]. The schematic diagram for the electromagnetic radiation and transmission of the return stroke is shown in Figure 8, where H is the height of the return-stroke channel, l is the distance between the B -field antenna and the return-stroke channel, v is the speed of the return stroke, and c is the speed of the electromagnetic wave in the air. The values of these physical parameters are as follows: the measured length of l is 80 m, c is 3×10^8 m/s, and H and v are assumed to be 8 km and 2×10^8 m/s, respectively. Since the observation distance of the B -field antenna is only 80 m in our experiment, the propagation effect over the finitely

conducting ground is not considered. Under this assumption, the expression for the B -field signal caused by the return stroke is as follows [24,25]:

$$B(t) = \frac{1}{2\pi\epsilon_0 c^2} \int_0^H \left(\frac{\sin \alpha(z')}{R^2(z')} i(z', t - \frac{R(z')}{c}) + \frac{\sin \alpha(z')}{cR(z')} \frac{\partial i(z', t - R(z')/c)}{\partial t} \right) dz' \quad (2)$$

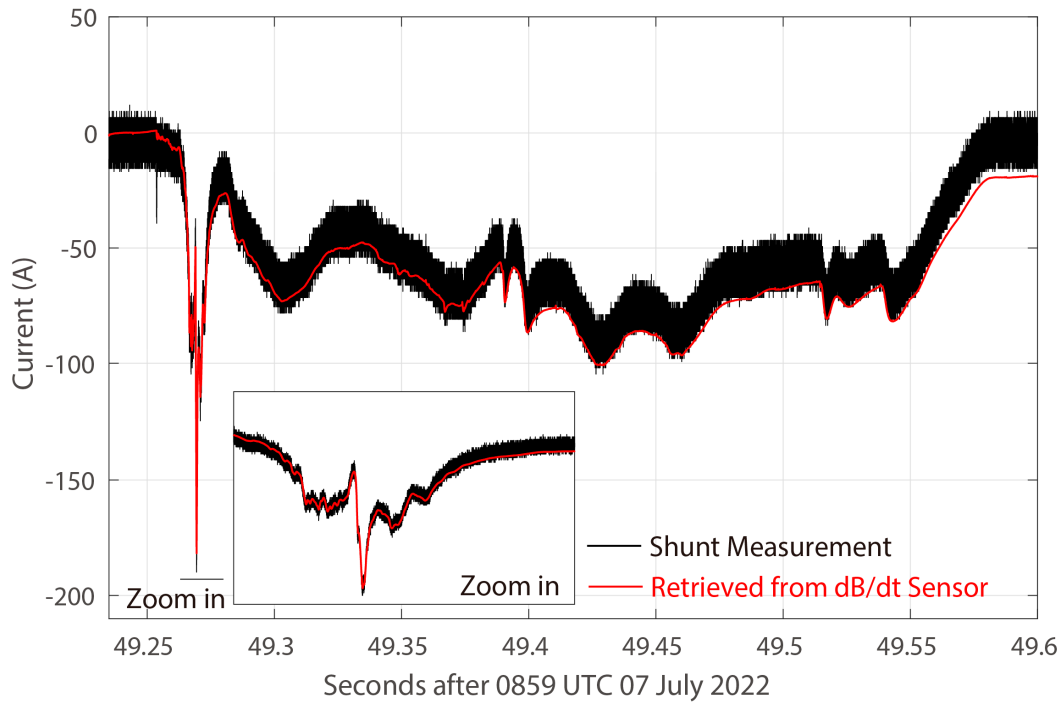


Figure 6. Comparison between the shunt measurement of ICC (black waveform) and the current waveforms reconstructed from the dB/dt antenna (red waveform) for the triggered lightning at 07:59:48 UTC on 7 July 2022 of the CMA-FEELS campaign.

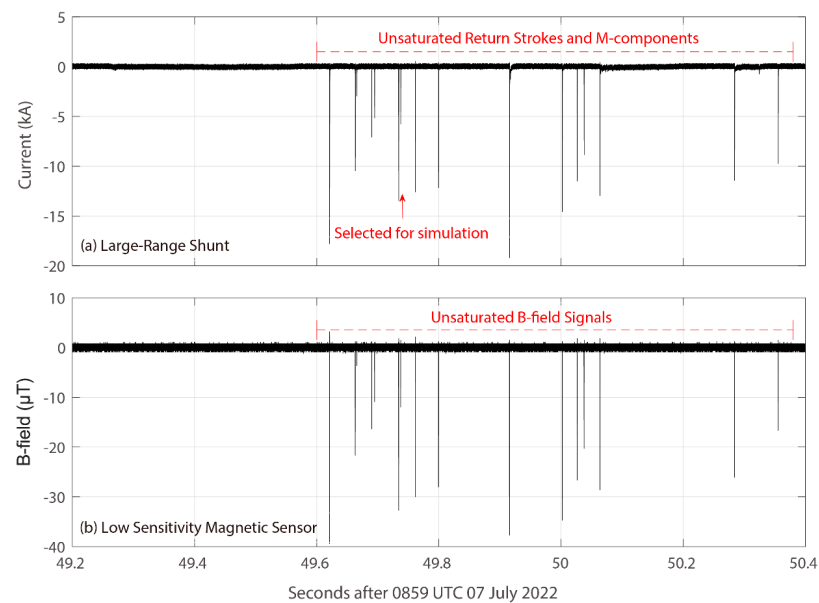


Figure 7. (a) Large-range current measured by the shunt and (b) B -field waveforms obtained by low-sensitivity antenna for the triggered lightning at 07:59:48 UTC on 7 July 2022 of the CMA-FEELS campaign.

The two terms on the right-hand side of Equation (2) are named as the induction component and the radiation component.

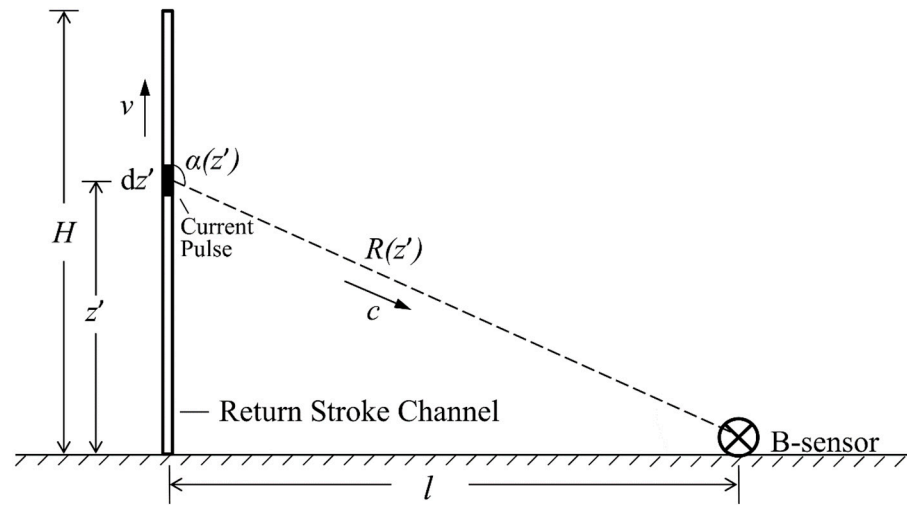


Figure 8. Schematic diagram for the electromagnetic radiation and transmission of return stroke.

In order to establish a quantitative relationship between the *B*-field measurement and the channel-base current during the stage of return stroke, the measured current should be put into the return-stroke model mentioned above for calculation. Note that the measured current is simulated by using the sum of two Heidler’s functions [26,27] for the convenience of the differential and integral operations. To eliminate the potential influence of the antenna range on the measurements, a return-stroke pulse with a smaller amplitude shown in Figure 7a (marked by the red arrow) is chosen for simulation. The function expression and corresponding parameter values for this return-stroke pulse are as follows:

$$i(t) = \frac{I_{01}}{\eta_1} \frac{\left(\frac{t}{\tau_{11}}\right)^{n_1}}{1 + \left(\frac{t}{\tau_{11}}\right)^{n_1}} e^{-\frac{t}{\tau_{12}}} + \frac{I_{02}}{\eta_2} \frac{\left(\frac{t}{\tau_{21}}\right)^{n_2}}{1 + \left(\frac{t}{\tau_{21}}\right)^{n_2}} e^{-\frac{t}{\tau_{22}}} \quad (3)$$

in which, $I_{01} = 5.08$ kA, $\tau_{11} = 0.25$ μ s, $\tau_{12} = 2.5$ μ s, $n_1 = 2$, $I_{02} = 3$ kA, $\tau_{21} = 2.1$ μ s, $\tau_{22} = 42$ μ s, $n_2 = 2$ and

$$\eta_1 = e^{-\left(\frac{\tau_{11}}{\tau_{12}}\right)(n_1 \frac{\tau_{12}}{\tau_{11}})^{\frac{1}{n_1}}}$$

$$\eta_2 = e^{-\left(\frac{\tau_{21}}{\tau_{22}}\right)(n_2 \frac{\tau_{22}}{\tau_{21}})^{\frac{1}{n_2}}}$$

The black waveform shown in Figure 9a presents the zoomed view of the return-stroke current pulse measured by shunt, and the red waveform is the simulation of this current pulse by using the function expression with the parameter values mentioned above; it can be seen that the simulation is in good agreement with the measurement. Furthermore, Figure 9b compares the measured *B*-field pulse (black waveform) radiated by the return stoke at 80 m range and the simulated *B*-field pulse (red waveform) at the same distance. The simulated *B*-field pulse is calculated by putting the simulated current pulse into the MTL return-stroke model, and its constitutions, i.e., the induction component (blue-dashed waveform) and radiation component (green-dashed waveform), are given separately. The comparison exhibits that for the falling edge of the *B*-field pulse, the simulated *B*-field pulse shows fairly good consistency with the measured one, but the two waveforms present a large deviation for the rising edge. Considering that the frequency below 4 kHz of *B*-field signals obtained by the low-sensitivity antenna is filtered during the measurement, we digitally filter the simulated *B*-field pulse over the same frequency band, and the filtered waveform (purple waveform) is also presented in Figure 9b. It can be seen that the simulated *B*-field pulse after filtering is very consistent with the measured one,

indicating that the high-pass filtering mainly affects the rising edge of the waveform. Based on the above analysis, a quantitative relationship has been established between the channel-base current and the measured B -field pulse of the return stroke. As illustrated in Figure 9b, the induction component is found to dominate the total magnetic field at this observation range, and it is reasonable to infer that the channel-base current and the associated B -field waveform exhibit consistency. Figure 9c presents a comparison between the two waveforms that have been normalized, which validates the aforementioned speculation. The result demonstrates the effectiveness of utilizing B -field measurement for retrieving the return stroke current, particularly in the range where the induction component dominates the total magnetic field.

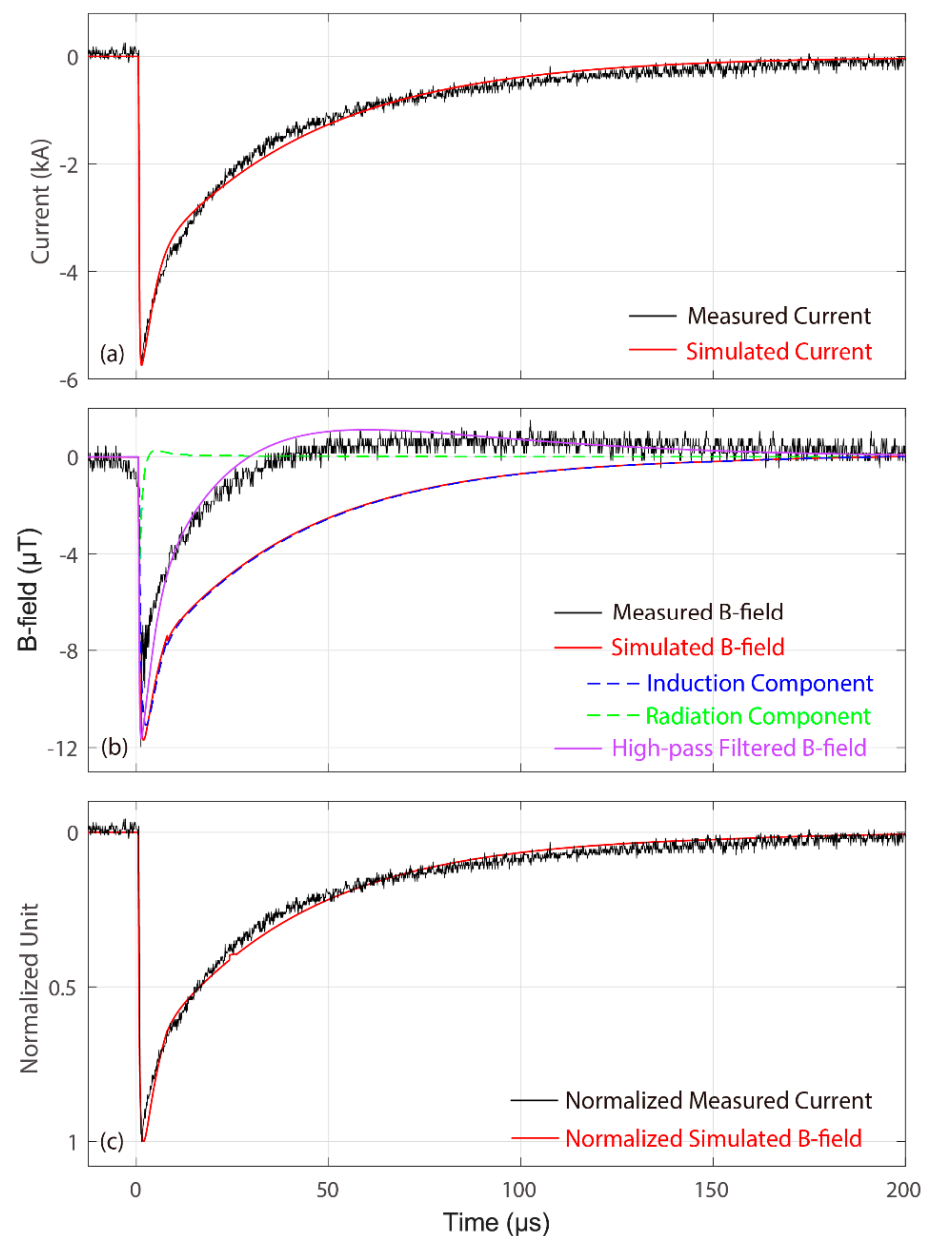


Figure 9. (a) Comparison between the measured (in black) and simulated (in red) current pulse of return stroke; (b) Comparison between the measured B -field pulse (in black), simulated B -field pulse (in red) and filtered simulated B -field pulse (in purple) of the return stroke, and also the induction component (in blue) and radiation component (in green) of the simulated B -field pulse; (c) Comparison between the measured current pulse (in black) and simulated B -field pulse (in red) of the return stroke that have been normalized.

4. Discussion

For natural lightning, it is difficult to obtain the current waveform for its random characteristics of lightning discharge. However, triggered lightning can reproduce the discharge process of natural lightning, especially for the continuous current and return strokes. Based on that, it is feasible to retrieve the natural lightning-current waveform or at least estimate its peak value by using the B -field antennas mentioned above, as long as the natural lightning occurs within a certain range.

The established quantitative relationship between the close-range B -field measurement and the channel-base current in the paper is based on the condition that the inductive field dominates the total magnetic field. Therefore, it is necessary to present the variation of the B -field components in the total field proportion with the observed distance. Figure 10 shows the variation curves of the correlation coefficients between the B -field components and the total field of the return stroke with distance. It is found that the correlation coefficient between the induction component and the total field of the return stroke is still above 0.7 when the observed distance is 1.5 km. Considering that the return stroke contains many more components with higher frequency than the continuous current (as shown in Figure 3), it is reasonable to determine that the magnetic fields generated by lightning discharge within 1.5 km are dominated by induction-field components, regardless of the impulsive discharge or the continuous discharge. Hence, for natural lightning occurring within 1.5 km, the B -field measurements obtained by the dB/dt antenna and the low-sensitivity antenna can be used to establish the quantitative relationship with the lightning current.

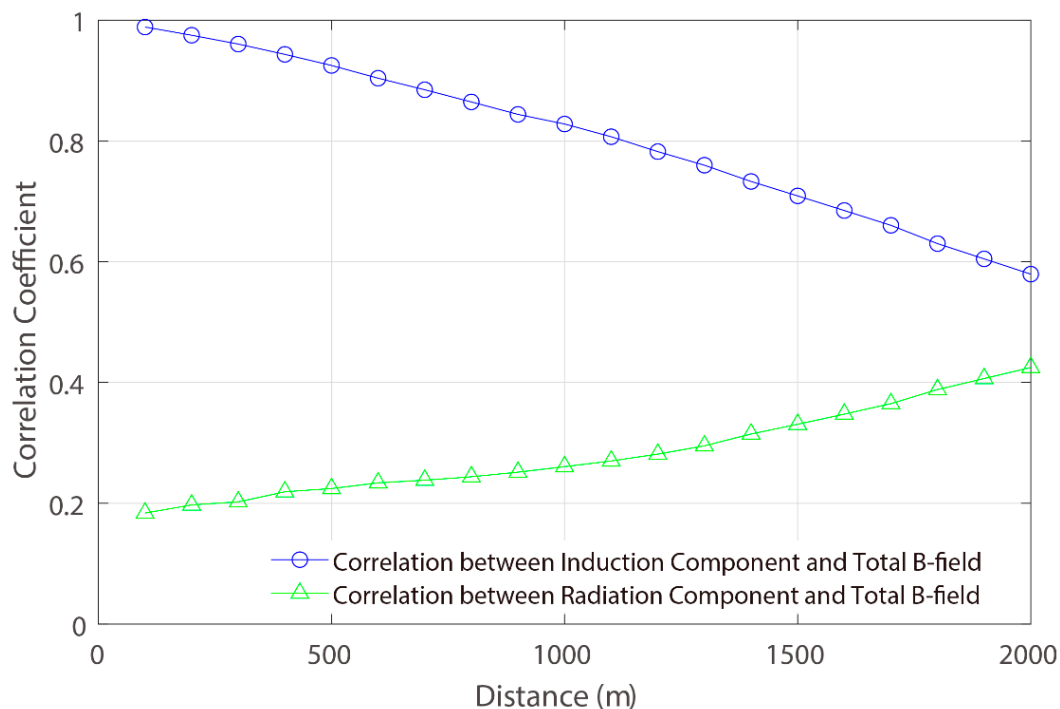


Figure 10. Variation curves of the correlation coefficients between the B -field components and the total field with distance.

For the inversion of ICC in Figure 6, its conversion coefficient $\beta(t)$ is determined by comparing the measured waveform with the inversion waveform. Even though the tortuosity of the channel above the trace of steel wire differs greatly in different triggered-lightning flashes, the conversion coefficient in Figure 6 is consistent with that in the SHATLE campaign, where the dB/dt antenna is deployed at similar distance from the rocket-launching site. The result confirms that the conversion coefficient is dominated by the distance between the dB/dt antenna and the rocket-launching site in the experiment. By deploying the dB/dt antenna at different places during the triggered-lightning experiment,

the conversion coefficients at different distances can be determined via comparing the measured waveform with the inversion waveform. Then a curve of conversion-coefficient variation with distance can be fitted. Based on the curve, the waveform of the natural return stroke that occurred within 1.5 km can be retrieved.

As shown in Figure 2, the upper limit of LF-MF antenna's dB/dt portion is about 20 kHz, much higher than that of the dB/dt antenna (8.5 kHz). Theoretically, the LF-MF antenna should also be useful for the inversion of the ICC waveform since the measurement contains more B -field signal with higher frequency. With the similar method described in Section 3.2, the B -field signals recorded by the LF-MF antenna at 80 m range are numerically integrated to reconstruct the ICC waveform (blue waveform in Figure 11) and are compared with the inversion waveform by using the dB/dt antenna (red waveform in Figure 11). The inset in Figure 11 shows the zoomed view of the ICV for the convenience of comparison. Not as expected, it shows significant differences for the current waveforms retrieved from the measurements of the two antennas. For the retrieved waveform from the LF-MF antenna, the fluctuations with lower frequency of ICC cannot be retrieved, but only the millisecond-scale variations. This is because the dB/dt portion of the LF-MF antenna bandwidth cannot cover the frequency below 500 Hz. In addition, some microsecond-scale variations are presented in the retrieved waveform, which are caused by the numerical integration of the signals within the 3-dB bandwidth of the LF-MF antenna. Since the B -field measurement noise with random distribution is cancelled mutually during the numerical integration, the noise levels for the two retrieved waveforms are very low. Based on the above analysis, we can learn that in order to optimize the retrieved waveform of ICC, the 3-dB portion of the dB/dt antenna should be as narrow as possible in the antenna design to reduce the influence of interference signals, and the lower cutoff frequency of the dB/dt portion should be closer to DC to ensure that more effective signals are involved in the numerical integration.

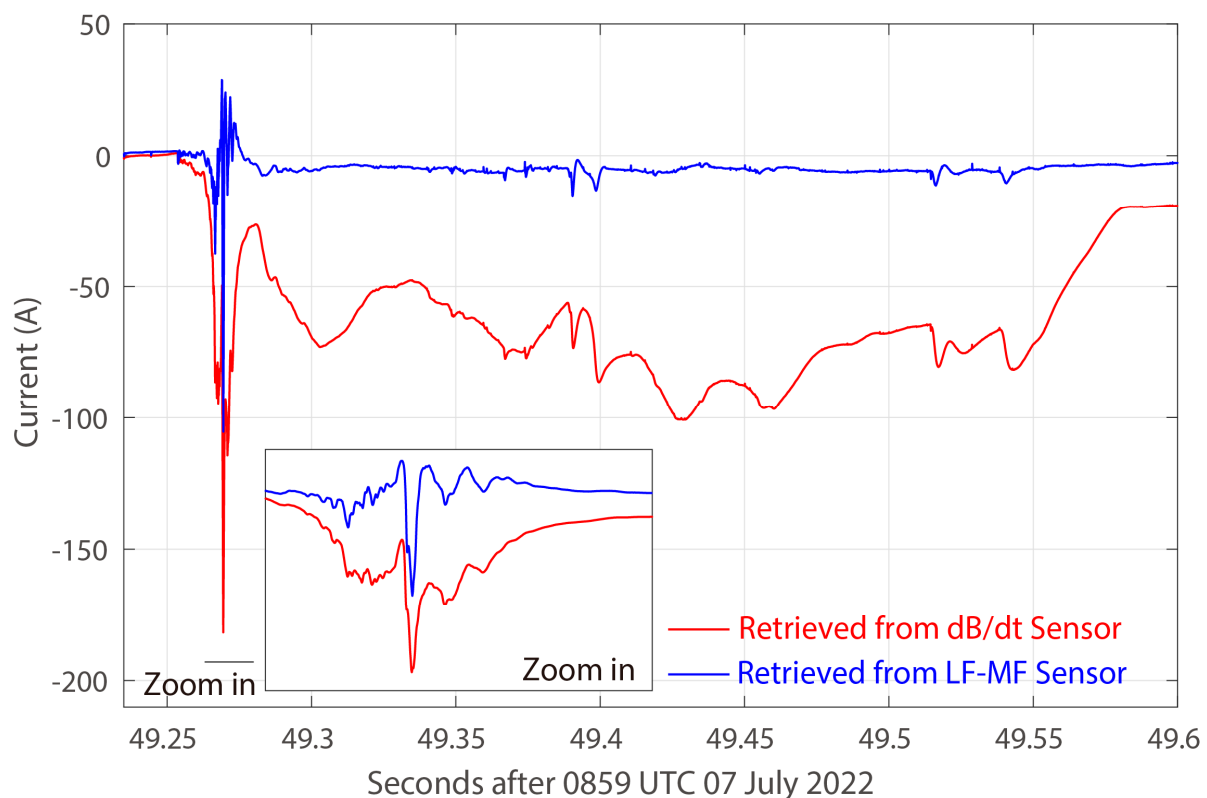


Figure 11. Comparison between the current waveforms reconstructed from the dB/dt antenna (red waveform) and the LF-MF antenna (blue waveform) for the triggered lightning at 07:59:48 UTC on 7 July 2022 of the CMA-FEBLS campaign.

The analysis in Section 3.3 demonstrates that the measured B -field pulse shows good consistency with the return-stroke current pulse, especially for the falling edge. Hence, the peak value of the return-stroke current could be estimated via the B -field measurement after the proportionality coefficient is determined. Figure 12 presents the proportionality coefficients between the B -field peak and the current peak for the 13 return strokes shown in Figure 7. The average proportionality coefficient is about 0.45 kA/nT, and the deviation ratio of each coefficient is also shown in Figure 12. It is found that the proportional relationship between the B -field peak and the current peak is very close, except for the 5th return stroke, for which the deviation ratio exceeds 10%. This is because the 5th return stroke caused the strongest discharge during this triggered lightning, and its associated B -field signal was saturated to some extent, making the measured peak value lower than the actual result. The proportionality coefficient can be also treated as a constant for the return stroke that occurred at a fixed distance. Therefore, by fitting a curve of the proportionality-coefficient variation with distance, the return-stroke current waveform of natural lightning that occurred within 1.5 km can be retrieved, or at least its peak value can be estimated.

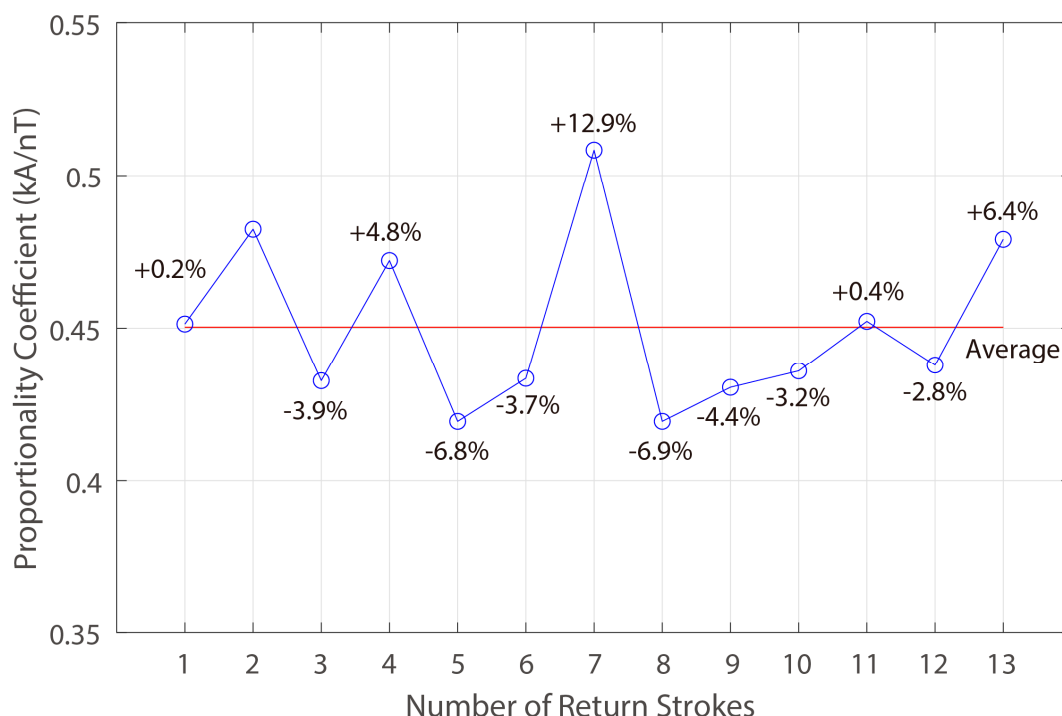


Figure 12. Proportionality coefficients between the B -field peak and the current peak for the 13 return strokes of the triggered lightning at 07:59:48 UTC on 7 July 2022 of the CMA-FEBSL campaign.

5. Summary

In order to establish a quantitative relationship between the close-range B -field signals and the channel-base current at different stages of triggered lightning, three B -field antennas with different frequency responses were deployed at about 80 m from the rocket launching site of the CMA-FEBSL in the summer of 2022. The three frequency-divided B -field antennas are named LF-MF antenna, dB/dt antenna and low-sensitivity antenna, respectively, according to the main frequency ranges and amplitudes obtained from the calibration curves. In this paper, the ICC waveform of the triggered lightning is reconstructed by numerically integrating the B -field signals measured with the dB/dt antenna, and the retrieved waveform shows fairly good agreement with the channel-base current recorded with the shunt. Even though the tortuosity of the channel above the trace of steel wire differs a great deal in different triggered-lightning flashes, the conversion coefficient is consistent with that in the SHATLE campaign, which proves the effectiveness of the method. For the current waveform retrieved from the measurements of the LF-MF antenna,

the fluctuations with a lower frequency of ICC cannot be retrieved, but only the millisecond-scale variations because the dB/dt portion of the LF-MF antenna bandwidth cannot cover the frequency below 500 Hz. In addition, some microsecond-scale variations are presented in the retrieved waveform, which is caused by the numerical integration of the signals within the 3-dB bandwidth of the LF-MF antenna. After the influence of the antenna bandwidth in the calculation is considered, the B -field signals of return stroke measured with the low-sensitivity antenna can be well simulated by putting the return-stroke current pulse into the MTLL model. It is found that the induction component dominates the total magnetic field when the observed distance is less than 1.5 km, and hence the return-stroke current and the associated B -field waveform exhibit consistency within the range. Based on that, for the natural return stroke that occurred within 1.5 km, its current waveform can be retrieved or at least its peak value can be estimated by using the B -field measurements.

Author Contributions: Conceptualization, Y.F. and Y.Z.; methodology, Y.F. and Y.Z.; software, Y.F.; validation, Y.F., Y.Z. and W.L.; formal analysis, Y.F.; investigation, Y.F., Y.Z., W.L., Y.M., B.W., Q.Q., D.Z., G.L. and A.W.; data curation, Y.F., Y.Z., W.L., Y.M., B.W., Q.Q., D.Z., G.L. and A.W.; writing—original draft preparation, Y.F.; writing—review and editing, Y.Z. and W.L.; project administration, W.L.; funding acquisition, Y.F., Y.Z. and W.L. All authors have read and agreed to the published version of the manuscript.

Funding: This research was funded by the National Natural Science Foundation of China (grant number 41905004), S&T Development Fund of CAMS (grant number 2023KJ050), Basic Research Fund of Chinese Academy of Meteorological Sciences (grant number 2021Z011), and the Science and Technology Foundation of Guizhou Province (grant number ZK[2022]245).

Data Availability Statement: The data can be obtained from the corresponding author (zhangyang@cma.gov.cn).

Acknowledgments: We are thankful to all members of the lightning group of the State Key Laboratory of Severe Weather, as well as Shaodong Chen and Xu Yan for their assistance with the experiments.

Conflicts of Interest: The authors declare no conflict of interest.

Abbreviations

CMA-FEBLS	Field Experiment Base on Lightning Sciences, China Meteorological Administration
GCOELD	Guangdong Comprehensive Observation Experiment on Lightning Discharge
SHATLE	SHAndong Triggering Lightning Experiment
B -field	magnetic field
E -field	electric field
UPL	upward positive leader
ICC	initial continuous current
MF	medium frequency (300 kHz–3 MHz)
LF	low frequency (30 kHz–300 kHz)
VLF	very low frequency (3 kHz–30 kHz)
SLF	super low frequency (30 Hz–300 Hz)
TL	transmission line
MTLL	modified transmission line model with linear current decay with height

References

1. Brook, M.; Kitagawa, N.; Workman, E.J. Quantitative study of strokes and continuing currents in lightning discharges to ground. *J. Geophys. Res.* **1962**, *67*, 649–659. [[CrossRef](#)]
2. Kodali, V.; Rakov, V.A.; Uman, M.A.; Rambo, K.J.; Schnetzer, G.H.; Schoene, J.; Jerauld, J. Triggered-lightning properties inferred from measured currents and very close electric fields. *Atmos. Res.* **2005**, *76*, 355–376. [[CrossRef](#)]
3. DeCarlo, B.A.; Rakov, V.A.; Jerauld, J.; Schnetzer, G.H.; Schoene, J.; Uman, M.A.; Rambo, K.J.; Kodali, V.; Jordan, D.M.; Maxwell, G.; et al. Distribution of Currents in the Lightning Protective System of a Residential Building-Part I: Triggered-Lightning Experiments. *IEEE Trans. Power Deliv.* **2008**, *23*, 2439–2446. [[CrossRef](#)]
4. Campos, L.Z.S.; Saba, M.M.F.; Pinto, O.; Maurício, G.B. Waveshapes of continuing currents and properties of M-components in natural positive cloud-to-ground lightning. *Atmos. Res.* **2009**, *91*, 416–424.

5. Newman, M.M.; Stahmann, J.R.; Robb, J.D.; Lewis, E.A.; Martin, S.G.; Zinn, S.V. Triggered lightning strokes at very close range. *J. Geophys. Res.* **1967**, *72*, 4671–4674. [[CrossRef](#)]
6. Schoene, J.; Uman, M.A.; Rakov, V.A.; Rambo, K.J.; Jerauld, J.; Mata, C.T.; Mata, A.G.; Schnetzer, G.H. Characterization of return-stroke currents in rocket-triggered lightning. *J. Geophys. Res.* **2009**, *114*, D03106. [[CrossRef](#)]
7. Thottappillil, R.; Goldberg, J.D.; Rakov, V.A.; Uman, M.A.; Fisher, R.J.; Schnetzer, G.H. Properties of M-components from currents measured at triggered lightning channel base. *J. Geophys. Res.* **1995**, *100*, 25711–25720. [[CrossRef](#)]
8. Fieux, R.; Gary, C.; Hubert, P. Artificially triggered lightning above land. *Nature* **1975**, *257*, 212–214. [[CrossRef](#)]
9. Fisher, R.J.; Schnetzer, G.H.; Thottappillil, R.; Rakov, V.A.; Uman, M.A.; Goldberg, J.D. Parameters of triggered-lightning flashes in Florida and Alabama. *J. Geophys. Res.* **1993**, *98*, 22887–22902. [[CrossRef](#)]
10. Lalande, P.; Bondiou-Clergerie, A.; Laroche, P.; Eybert-Berard, A.; Berlandis, J.-P.; Bador, B.; Bonamy, A.; Uman, M.A.; Rakov, V.A. Leader properties determined with triggered lightning techniques. *J. Geophys. Res.* **1998**, *103*, 14109–14115. [[CrossRef](#)]
11. Willett, J.C.; Davis, D.A.; Laroche, P. An experimental study of positive leaders initiating rocket-triggered lightning. *Atmos. Res.* **1999**, *51*, 189–219. [[CrossRef](#)]
12. Biagi, C.J.; Jordan, D.M.; Uman, M.A.; Hill, J.D.; Beasley, W.H.; Howard, J. High-speed video observations of rocket-and-wire initiated lightning. *Geophys. Res. Lett.* **2009**, *36*, L15801. [[CrossRef](#)]
13. Biagi, C.J.; Uman, M.A.; Hill, J.D.; Jordan, D.M. Observations of the initial, upward-propagating, positive leader steps in a rocket-and-wire triggered lightning discharge. *Geophys. Res. Lett.* **2011**, *38*, L24809. [[CrossRef](#)]
14. Wang, D.; Rakov, V.A.; Uman, M.A.; Fernandez, M.I.; Rambo, K.J.; Schnetzer, G.H.; Fisher, R.J. Characterization of the initial stage of negative rocket-triggered lightning. *J. Geophys. Res.* **1999**, *104*, 4213–4222. [[CrossRef](#)]
15. Thottappillil, R.; Rakov, V.A.; Uman, M.A. Distribution of charge along the lightning channel: Relation to remote electric and magnetic fields and to return-stroke models. *J. Geophys. Res.* **1997**, *102*, 6987–7006. [[CrossRef](#)]
16. Qie, X.; Zhao, Y.; Zhang, Q.; Yang, J.; Feng, G.; Kong, X.; Zhou, Y.; Zhang, T.; Zhang, G.; Zhang, T.; et al. Characteristics of triggered lightning during Shandong artificial triggering lightning experiment (SHATLE). *Atmos. Res.* **2009**, *91*, 310–315. [[CrossRef](#)]
17. Jiang, R.; Qie, X.; Wang, C.; Yang, J. Propagating features of upward positive leaders in the initial stage of rocket-triggered lightning. *Atmos. Res.* **2013**, *129*, 90–96. [[CrossRef](#)]
18. Fan, Y.; Lu, G.; Jiang, R.; Zhang, H.; Li, X.; Liu, M.; Qie, X.; Zheng, D.; Lyu, W.; Zhang, Y.; et al. Characteristics of electromagnetic signals during the initial stage of negative rocket-triggered lightning. *J. Geophys. Res. Atmos.* **2018**, *123*, 11625–11636. [[CrossRef](#)]
19. Fan, Y.; Lu, G.; Li, X.; Zheng, T.; Zhang, H.; Jiang, R.; Liu, M.; Qie, X.; Zhang, Y.; Zhang, Y.; et al. Measurements of magnetic pulse bursts during initial continuous current of negative rocket-triggered lightning. *J. Geophys. Res. Atmos.* **2019**, *124*, 11710–11721. [[CrossRef](#)]
20. Lu, G.; Fan, Y.; Zhang, H.; Jiang, R.; Liu, M.; Qie, X.; Cummer, S.A.; Han, C.; Liu, K. Measurement of continuing charge transfer in rocket-triggered lightning with low-frequency magnetic sensor at close range. *J. Atmos. Sol.-Terr. Phys.* **2018**, *175*, 76–86. [[CrossRef](#)]
21. Zheng, D.; Zhang, Y.; Lu, W.; Zhang, Y.; Dong, W.; Chen, S.; Dan, J. Characteristics of return stroke currents of classical and altitude triggered lightning in GCOELD in China. *Atmos. Res.* **2013**, *129–130*, 67–68. [[CrossRef](#)]
22. Zhang, Y.; Yang, S.; Lu, W.; Zheng, D.; Dong, W.; Li, B.; Chen, S.; Zhang, Y.; Chen, L. Experiments of artificially triggered lightning and its application in Conghua, Guangdong, China. *Atmos. Res.* **2014**, *135–136*, 330–343. [[CrossRef](#)]
23. Rakov, V.A.; Dulzon, A. A modified transmission line model for lightning return stroke field calculations. In Proceedings of the 9th International Symposium on EMC, Zurich, Switzerland, 5–10 March 1991.
24. Uman, M.A.; McLain, D.K.; Krider, E.P. The electromagnetic radiation from a finite antenna. *Am. J. Phys.* **1975**, *43*, 33–38. [[CrossRef](#)]
25. Thottappillil, R.; Rakov, V.A. On different approaches to calculating lightning electric fields. *J. Geophys. Res.* **2001**, *106*, 14191–14206. [[CrossRef](#)]
26. Heidler, H. Analytische Blitzstromfunktion zur LEMP-Berechnung. In Proceedings of the 18th International Conference on Lightning Protection, Munich, Germany, 16–20 September 1985.
27. Rachidi, F.; Janischewskyj, W.; Hussein, A.M.; Nucci, C.A.; Guerrieri, S.; Kordi, B.; Chang, J.S. Current and electromagnetic field associated with lightning-return strokes to tall towers. *IEEE Trans. Electromagn. Compat.* **2001**, *43*, 356–367. [[CrossRef](#)]

Disclaimer/Publisher’s Note: The statements, opinions and data contained in all publications are solely those of the individual author(s) and contributor(s) and not of MDPI and/or the editor(s). MDPI and/or the editor(s) disclaim responsibility for any injury to people or property resulting from any ideas, methods, instructions or products referred to in the content.